Clays and Clay Minerals, Vol. 64, No. 4, 413–424, 2016.

STABILITY OF THE HYDRONIUM CATION IN THE STRUCTURE OF ILLITE

ELIZABETH ESCAMILLA-ROA[1], FERNANDO NIETO[1,2], AND C. IGNACIO SAINZ-DÍAZ[1,*]

[1] Instituto Andaluz de Ciencias de la Tierra (CSIC-University of Granada), Av. de las Palmeras 4, 18100 Armilla, Granada (Spain)
[2] Departamento de Mineralogía y Petrología, Universidad de Granada, Avenida Fuentenueva, 18002 Granada, Spain

Abstract—Some aspects of the crystal structure of illite are not understood properly yet, in spite of its abundance and significance as a component of soils, sediments, and low-grade metamorphic rocks. The present study aimed to explore the role of hydronium cations in the interlayer space of illite in a theoretical-experimental approach in order to clarify previous controversial reports. The infrared spectroscopy of this mineral has been studied experimentally and by means of atomistic calculations at the quantum mechanical level. The tetrahedral charge is critical for the stability of the hydronium cations, the presence of which has probably been underestimated in previous studies. In the present study, computational studies have shown that the hydronium cations in aqueous solutions are likely to be intercalated in the interlayer space of illite, exchanging for K cations. During the drying process these cations are stabilized by hydrogen bonds in the interlayer space of illite.

Key Words—DFT, Hydrogen Bond, Hydronium, Illite, IR spectroscopy, Phyllosilicate.

INTRODUCTION

Illite is a 2:1 dioctahedral phyllosilicate which could be classified somewhere between clays and mature mica. In spite of its abundance in sediments, its crystal structure is poorly understood due to the high degree of disorder in stacking of its layers, cation substitutions, cation arrangements along each sheet, and the small size of its crystalline domain. The chemical composition of illite is similar to that of smectite but has different properties: illite is non-swelling and has a smaller cation exchange capacity. In general, illite has a certain tetrahedral charge which is greater than that of smectites and less than that of more mature micas, with K^+ as the most common interlayer cation.

According to the International Mineralogical Association (Rieder *et al.*, 1998), the term illite is given to interlayer-cation-deficient mica with <0.85 interlayer atoms per formula unit. The mechanism of charge compensation in these minerals is controversial, however. The presence of hydronium cations to compensate the charge deficiency was proposed by Brown and Norrish (1952). On the contrary, Hower and Mowatt (1966) proposed that no hydronium cation compensation occurs.

Spectroscopic studies have been used widely to explore the structure of the phyllosilicates and interlayer water (Bishop *et al.*, 1994; Fialips *et al.*, 2002). The supramolecular network of water molecules in a nano-space, such as the interlayer space of phyllosilicates, is difficult to understand, however (Kuligiewicz *et al.*, 2015). Discrepancies related to the detection (by infrared, IR, spectroscopy) of the hydronium cation in phyllosilicates have been reported (White and Burns, 1963). Most of the experimental studies of this target are based on crystallographic and spectroscopic approaches that are closely related to the atom positions and atomic vibrations. Molecular modeling calculations, based on atoms and molecules, may, therefore, be a useful complementary tool for helping to understand this phenomenon. This theoretical approach has been applied to clay minerals in recent decades with satisfactory results in terms of crystallographic (Escamilla-Roa *et al.*, 2013; Sainz-Díaz *et al.*, 2003) and spectroscopic (Escamilla-Roa *et al.*, 2014) properties.

The behavior of water in nanoconfined spaces is not well understood, especially in the interlayer space of phyllosilicates. The role of water in the interlayer space is critical in the cation exchange process. Several computational studies on the behavior of water in the interlayer space of phyllosilicates have been reported (Michot *et al.*, 2012; Morrow *et al.*, 2013; Wang *et al.*, 2005). The study of the structure and properties of H_3O^+ ions in the interlayer sheet is important for exploring crystallographic and physical-chemical properties of illite, and contributes to an understanding of the stability of H_3O^+ ions in the interlayer space. The present work was based on the hypothesis of the existence of the hydronium cation in the interlayer space of illite and the objective was to study the stability of and effect of H_3O^+ as an interlayer cation (IC) on the illite structure with and without water molecules.

* E-mail address of corresponding author:
ignacio.sainz@iact.ugr-csic.es
DOI: 10.1346/CCMN.2016.0640406

This paper is published as part of a special issue on the subject of 'Computational Molecular Modeling'. Some of the papers were presented during the 2015 Clay Minerals Society-Euroclay Conference held in Edinburgh, UK.

METHODOLOGY

Several theoretical models have been explored in attempts to understand the stability of hydronium cations in the interlayer space of illites. Ultimately, theoretical and experimental studies have merged together to elucidate spectroscopic properties.

Sample

Illite IMt-2, from the Cambrian shales from Silver Hill, Jefferson Canyon, Montana, USA, was obtained from the Source Clays Repository of The Clay Minerals Society. A full description was reported by Hower and Mowatt (1966). The <2 mm fraction of this illite was separated by suspension in water and centrifugation. No further chemical treatment was applied during the separation process. The sample was air-dried and disaggregated gently using an agate pestle and mortar.

Spectroscopic experiments

A Fourier-transform Infrared (FTIR) spectrophotometer (model JASCO 6200A) located at the University of Granada (Spain) was used with an Attenuated Total Reflection (ATR) accessory. Spectra were analyzed by means of the *SpectraManager* program (provided by JASCO).

Calculations

First-principles total energy calculations based on Density Functional Theory (DFT) were performed with the Generalized Gradient Approximation (GGA) and the Perdew, Burke, and Ernzerhof (PBE) exchange correlation functional (Perdew *et al.*, 1996). The *Dmol3* program was used, implemented in the *Materials Studio* (MS) package, including periodical boundary conditions (Accelrys, 2009). The electronic calculations were performed with a double-zeta basis set augmented with polarization functions (DNP) with Semi-core Pseudopotentials (DSPP). The convergence criterion for the self-consistent field was 1×10^{-5} Ha (Hartrees, 1 Ha = 627.51 kcal/mol). The optimization of geometries of different structures was performed at 0 K. The harmonic vibration frequencies were calculated diagonalizing the mass-weighted second-derivative Hessian matrix.

Experimental atomic coordinates for the crystal structure of illites were taken from the models proposed by Drits *et al.* (1984) based on oblique-texture electron diffraction studies of dioctahedral smectites. The H atom coordinates were taken from the previous study of Giese (1979), where they were optimized by means of interatomic empirical potential calculations (Sainz-Diaz *et al.*, 2001). The illite model is in the *trans*-vacant crystal form, and of 1*M* polytype. From an experimental composition of $[(Si_{3.4}Al_{0.6})(Al_{1.47}Fe^{3+}_{0.19}Fe^{2+}_{0.06}Mg_{0.28})K_{0.69}Na_{0.01}(OH)_2O_{10}]$ (Nieto *et al.*, 2010), a model of $[(Si_{3.25}Al_{0.75})(Al_{1.75}Mg_{0.25})K(OH)_2O_{10}]$ was created. This model allows the generation of a $2 \times 1 \times 1$ supercell of 84 atoms without fractional cation substitution with periodic boundary conditions $(Si_{13}Al_3)(Al_7Mg_1)K_4(OH)_8O_{40}$. To study the stability of the hydronium ion in the illite interlayer space, one K^+ was substituted by one H_3O^+ cation in the interlayer space $(Si_{13}Al_3)(Al_7Mg_1)K_3(H_3O)(OH)_8O_{40}$. Hydrated systems were also simulated with varying amounts of water in the interlayer space surrounding the interlayer cations.

To compare the energy of these cations in the interlayer space with a dissolution environment, boxes of mixtures of water and several ions (H_3O^+, HO^-, K^+) were generated applying periodical boundary conditions by using the amorphous cell-builder modulus based on Monte Carlo simulations with geometry optimization for refinement, using the Compass Force Field at 298 K and a density of 1 g/cm^3 implemented in *Materials Studio* (Accelrys, 2009). Further optimizations of these models were performed at the DFT level.

RESULTS AND DISCUSSION

Dry K-illite model

Initially, the dry model of illite, without water or hydronium molecules, was calculated with the composition $[(Si_{3.25}Al_{0.75})(Al_{1.75}Mg_{0.25})K(OH)_2O_{10}]$, with tetrahedral and octahedral charges and only K^+ as the interlayer cation. This model can be considered as 'a near muscovitic composition' with some excess Si that is compensated by a substitution of Al by Mg in the octahedral sheet, *i.e.* a Tschermaks/phengitic substitution, which is common in illite and in micas generally. A similar structure was optimized in preliminary calculations (Sainz-Díaz *et al.*, 2005), yielding a crystal lattice with the cell parameters a = 5.29, b = 9.15, c = 10.07 Å, α = 90.0º, β = 101.75º, and γ = 90.0º. These parameters are consistent with the experimental values of smectites and only slightly different from the experimental crystal lattice parameters of illite IMt-2: a = 5.20–5.24, b = 9.01–9.06, c = 10.13–10.17 Å, and β = 101.3–101.8º (Nieto *et al.*, 2010).

A $2 \times 1 \times 1$ supercell was created that corresponds to the formula $(Si_{13}Al_3)(Al_7Mg_1)K_4(OH)_8O_{40}$, where the tetrahedral Al occurs in different sheets of the same layer, two in one sheet and another in the other tetrahedral sheet, being maximally dispersed along the tetrahedral sheet (Sainz-Díaz *et al.*, 2005) (Figure 1). All atomic positions were fully optimized at constant volume maintaining the above theoretical cell parameters. The distortion produced by the coupling of the tetrahedral and octahedral sheets means that the hexagons formed by Si oxide tetrahedrons change from hexagonal to ditrigonal symmetry with a certain angular freedom. In the optimized structure, the K cations remain in the center of the interlayer space. The K distances to the basal tetrahedral O atoms are slightly shorter (2.79–3.03 Å), however, in the sites with more

https://doi.org/10.1346/CCMN.2016.0640406 Published online by Cambridge University Press

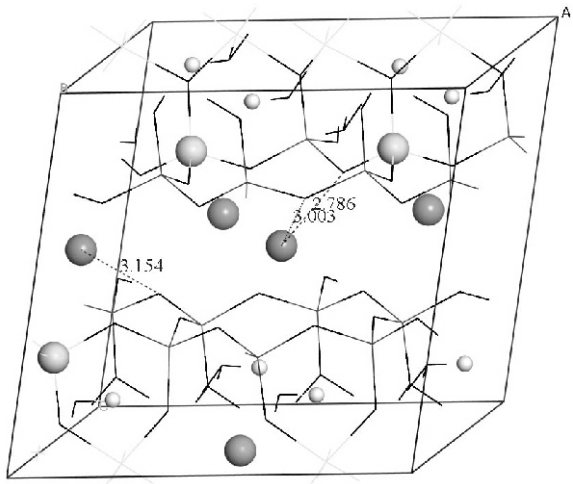

Figure 1. Optimized crystal structure of illite in completely dry conditions (view from the (010) plane). Some interatomic distances (Å) are included. The H, Al, Mg, Si, O, and K atoms are represented in white, light-gray, gray, light-gray, black, and dark-gray, respectively. The H, ^{IV}Al, Mg, and K atoms are highlighted in spheres. This graphical style is also applied to figures 2–4.

tetrahedral Al cations than in those with less Al (3.15–3.57 Å), due to the greater charge in the layer with more ^{IV}Al cations. The Mg substitution produces an additional negative charge in the axial O atoms joined to them, these being the Hirschfeld charges (Accelrys, 2009) of the O atoms (−0.316) which are greater than in other axial O atoms (−0.286). This Mg substitution has a similar effect on both tetrahedral sheets in a periodical crystal lattice, however. The Hirschfeld charges of the basal tetrahedral O atoms joined to the ^{IV}Al substitutions (−0.331, −0.340) are greater than in other basal O atoms (−0.266, −0.271). Hence, the electrostatic interaction of the K^+ cations is stronger with these basal O atoms with higher charges.

Hydronium K-illite

Previous thermogravimetry (TGA) studies of illite (Nieto *et al.*, 2010) suggested that after heating up to 138ºC, most of the water molecules were released from the interlayer space and only H_3O^+ remained in the structure. In such a scheme, the exchange of one K^+ cation by one hydronium cation per $2 \times 1 \times 1$ supercell was simulated, placing the new cation in different positions of the interlayer space: in the 'hexagonal' cavity in the tetrahedral sheet with octahedral Mg^{2+} substitution and without a tetrahedral substitution (model K_3H_3O*a*), in the cavity of the tetrahedral sheet with octahedral Mg^{2+} substitution and tetrahedral Al substitutions (model K_3H_3O*b*), and in the center of the interlayer space (model K_3H_3O*c*). All atomic positions were optimized at constant volume with the same cell parameters as in the former model.

After the optimization of model K_3H_3O*a*, the geometry of the structure changed (Table 1). In spite of the strong H bonds of the hydronium H atoms and the basal tetrahedral O atoms of the initial model, the repulsion between O atoms of hydronium and tetrahedral cavity triggers, during the optimization, the displacement of the H_3O^+ cation outside of the ditrigonal cavity toward the center of the interlayer space. In this structure, the hydronium cation is stabilized by H bonds and electrostatic interactions with the surrounding basal tetrahedral O atoms, H_2OH...Ob. The strongest interactions occur with the O atoms with high charge generated by the Al^{3+} tetrahedral substitution, where the Hirschfeld net charges of these O atoms (−0.330, −0.326 before approach by the hydronium cation) are greater than other O atoms (−0.260). Note that the charges of the O atoms close to the $^{IV}Al^{3+}$ decrease (−0.29, −0.25) when strong H bonds are formed with hydronium cations. The hydronium H atoms then form the shortest H bonds, $d(H_2OH^+...Ob)$ = 1.43 Å, with the basal O atom joined to one $^{IV}Al^{3+}$ substitution and to the

Table 1. The main hydrogen bonds (Å) of the hydronium ion within illite in dry and hydrated models. Structural formulae on the basis of $O_{40}(OH)_8$.

	Model					
Distance	K_3H_3O*a*	K_3H_3O*b*	K_3H_3O*c*	K_4w_3	$K_3H_3Ow_3$	$K_7(H_3O)_3w_6$
$H_3O...Ob_{T1}$ [a]	1.61	1.55			1.70	
$H_3O...Ob_{T2}$ [a]	1.43	1.42				
$H_3O...Ob_{T3}$ [a]	1.81, 2.72	2.57, 2.25	2.19, 2.20		1.62–2.00	1.34–2.79
$XOH...OH_2$ [b]			1.34		1.36	1.41
$HOH...OH_2$				2.47	2.85–3.32	2.29, 2.80
$K...OH_2$				2.96–3.5	2.68–3.18	2.67–3.27
ΔE [c]	0.0	5.83	9.02			

[a] Ob_{T1} and Ob_{T2}: basal O atoms joined to $^{IV}Al^{3+}$ cations along the direction of the *b* and *a* axes, respectively; Ob_{T3}: basal O atoms not close to an $^{IV}Al^{3+}$ cation.
[b] *X* = Si, H_2 of H_3O^+.
[c] ΔE is the relative energy with respect to K_3H_3O*a* (kcal/mol).

https://doi.org/10.1346/CCMN.2016.0640406 Published online by Cambridge University Press

Si cation placed between two $^{IV}Al^{3+}$ substitutions along the crystallographic *a* axis, AlOSiOAl, and another H bond at 1.61 Å with the basal O atom joined to other $^{IV}Al^{3+}$ substitution. This H bond is slightly longer because the basal O is joined to a Si cation with only one vicinal $^{IV}Al^{3+}$ substitution along the crystallographic *b* axis, sequence AlOSiOSi. A third hydrogen bond is observed with one basal oxygen atom of the other tetrahedral sheet, $d(H_2OH^+...Ob)$ = 1.81 Å (Figure 2a).

The optimization of model K_3H_3O*b* yielded similar behavior, the hydronium cation displaced from the tetrahedral cavity toward the center of interlayer space. The distance between the hydronium H atom and the octahedral OH group ($H_2OH^+...O$ of AlOHMg) is enlarged from the initial 1.73 Å to 3.16 Å after optimization, due to the repulsive interaction of the strong charge of the tetrahedral O atoms with the O atom of H_3O^+ (Figure 2b). This optimized structure is stabilized by H bonds and electrostatic interaction with basal tetrahedral O atoms. The Al^{3+} substitution that increased the negative O charge (Hirschfeld charges −0.331, −0.326) and the approach of the hydronium cation causes the formation of H bonds ($H_2OH^+...Ob_t$) with these basal O atoms. The strongest H-bond interactions are formed between the hydronium H atoms and the basal O atoms joined to these Al^{3+} substitutions at 1.42 and 1.55 Å (Table 1) as in the former model. The atomic charges of these O atoms decreased slightly (Hirschfeld charges −0.274, −0.287, respectively) due to the effect of the H bonds.

During the optimization of model K_3H_3O*c* the H_3O^+ cation remained in the center of the interlayer space forming a H bond with one basal tetrahedral O atom joined to a tetrahedral Al substitution (greater charge density). This H atom was finally transferred to the basal O atom joined to the Al^{3+} substitution. The result of this protonation is a new AlOHSi silanol group with a long bond length, *d*(OH) = 1.12 Å and a strong hydrogen bond (1.34 Å) with the O atom of the resulting water molecule (Figure 2c). The disposition of the H atoms in this complex hydronium-silanol maintains the relative geometry of the bond angles of hydronium cation. The behavior of this model can be due to the relative conformation of the hydronium H atoms in the interlayer space, where only one H atom is oriented directly toward a basal O atom with high charge, forming a Brönsted center.

In spite of this dissociation of the hydronium cation, this structure is not the most stable, whereas the model K_3H_3O*a* has the lowest energy (Table 1). The combination of several H bonds and electrostatic interactions probably has more effect than the dissociation of one H atom.

Hydrated model of illite

In order to understand the role of water molecules and hydronium cations, as a result of replacement of K^+ by H_3O^+ cation in the illite interlayer space, the presence of water molecules was also considered in these models. Previous experimental analysis of the illite sample in question determined an initial interlayer water content of 2.79% (Nieto *et al.*, 2010). Taking into account this amount of water and the quartz content, 92.21% of the illite can be considered as 'hosting' the interlayer water. This amount of water can, thus, correspond to the presence of 2.7 water molecules per supercell and two wet models were prepared with three water molecules per $(2 \times 1 \times 1)$ supercell: $[(Si_{13}Al_3)(Al_7Mg)K_4(OH)_8O_{40}(H_2O)_3]$ (K_4w_3) (Figure 3) and $(Si_{13}Al_3)(Al_7Mg)K_3(H_3O^+)(OH)_8O_{40}(H_2O)_3$ $(K_3H_3Ow_3)$ (Figure 4). Illite does not expand when placed in water, nor does it collapse with heating; this amount of water will, therefore, solvate partially the interlayer cations without increasing the interlayer spacing and no additional stress is created.

All atomic positions of both models were optimized at constant volume with the experimental cell parameters (a = 5.24, b = 9.06, c = 10.17 Å, and β = 101.75º) (Nieto *et al.*, 2010). After the optimization process, the K_4w_3 model showed the IC in the center of interlayer space and the water molecules solvating the IC, the average distance of the interaction is *d*(K...OH) = 3.19 Å. Only two water molecules show hydrogen bond interactions at 2.47 Å with each other. The major interactions of water molecules are with several basal O atoms of the tetrahedral sheet by hydrogen bonds ($HOH...O_b$), the range of the distances is between 1.49 and 2.74 Å (Figure 3).

When one K^+ is substituted by the hydronium cation, in the $K_3H_3Ow_3$ model, the hydronium cation does not remain in the center of the interlayer space during the optimization process. One proton of the initial H_3O^+ is transferred to a vicinal tetrahedral basal O atom. A new AlSiOH group and a water molecule are thus formed, and both are associated, forming a complex with a $d(SiO-H)$ = 1.14 Å and a strong hydrogen bond $d(H_2O...HOSi)$ = 1.36 Å. Such behavior is similar to that of the model K_3H_3O*c*, where this site is more reactive due to the high charge generated by the Al^{3+} tetrahedral substitution (Figure 4). The AlSiOH group is very important in the acidity-site concept that is related to reactivity. This site is known as a Brönsted acid site, which is produced by Si−O groups, the oxygen atoms of which are close to Al atoms, increasing the proton affinities. This behavior was observed in theoretical adsorption studies on amorphous silica and clays (Benco and Tunega, 2009; Leydier *et al.*, 2015).

After drying this sample at T < 138ºC, 1.5% of the water-hydronium content remained in the interlayer space (Nieto *et al.* 2010). Taking into account this amount of water-hydronium and the quartz content, 93.5% of illite was considered as hosting the water-hydronium in the interlayer space. This amount of water-hydronium corresponds, therefore, to the presence of

https://doi.org/10.1346/CCMN.2016.0640406 Published online by Cambridge University Press

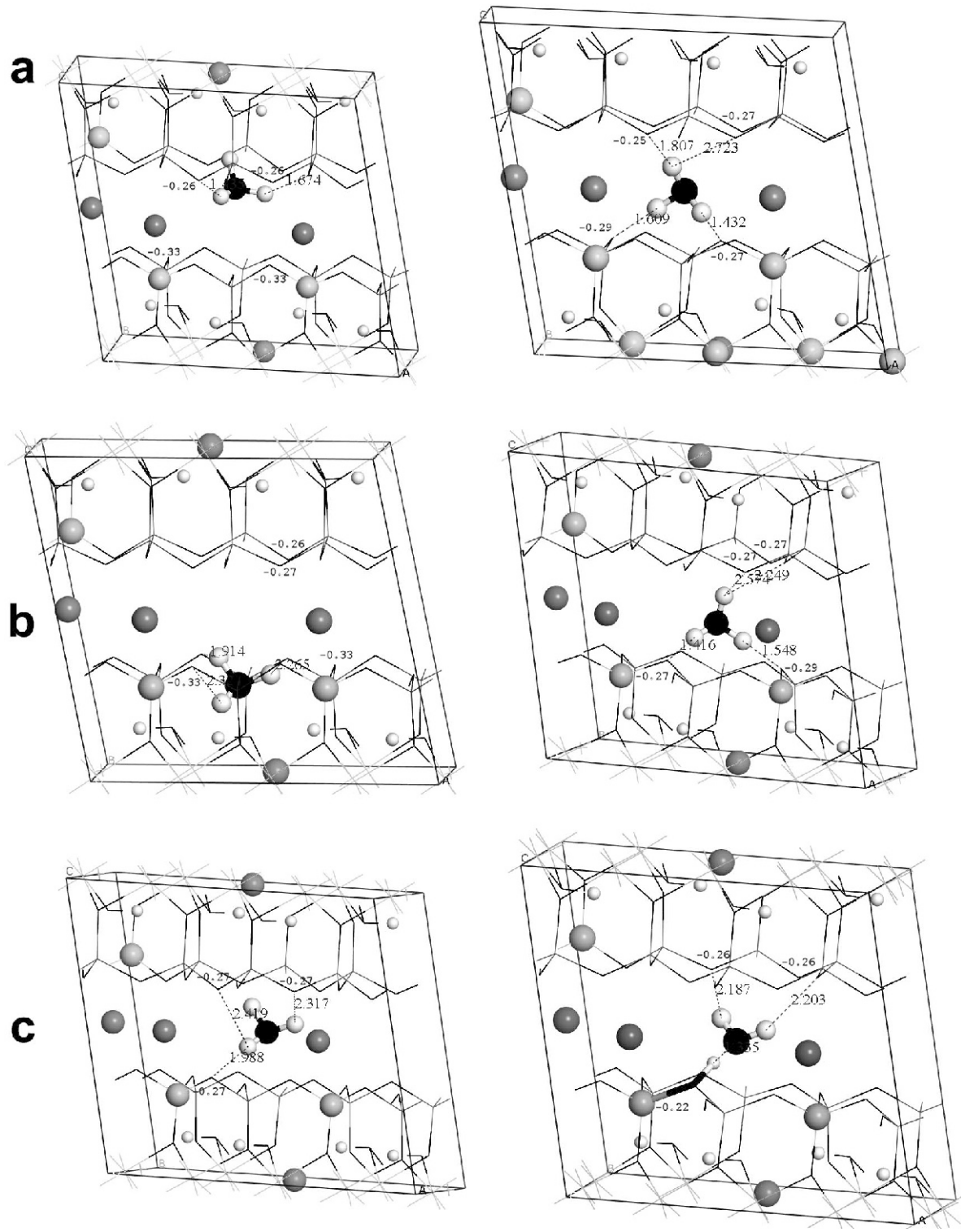

Figure 2. Initial (left side) and optimized (right side) structures of illite with hydronium cations (highlighted using balls) in the interlayer space without water molecules: models K_3H_3O*a* (a), K_3H_3O*b* (b), and K_3H_3O*c* (c). Atomic Hirschfeld net charges of some main O atoms and interatomic distances (Å) of H atoms of hydronium cations with basal O atoms are included.

https://doi.org/10.1346/CCMN.2016.0640406 Published online by Cambridge University Press

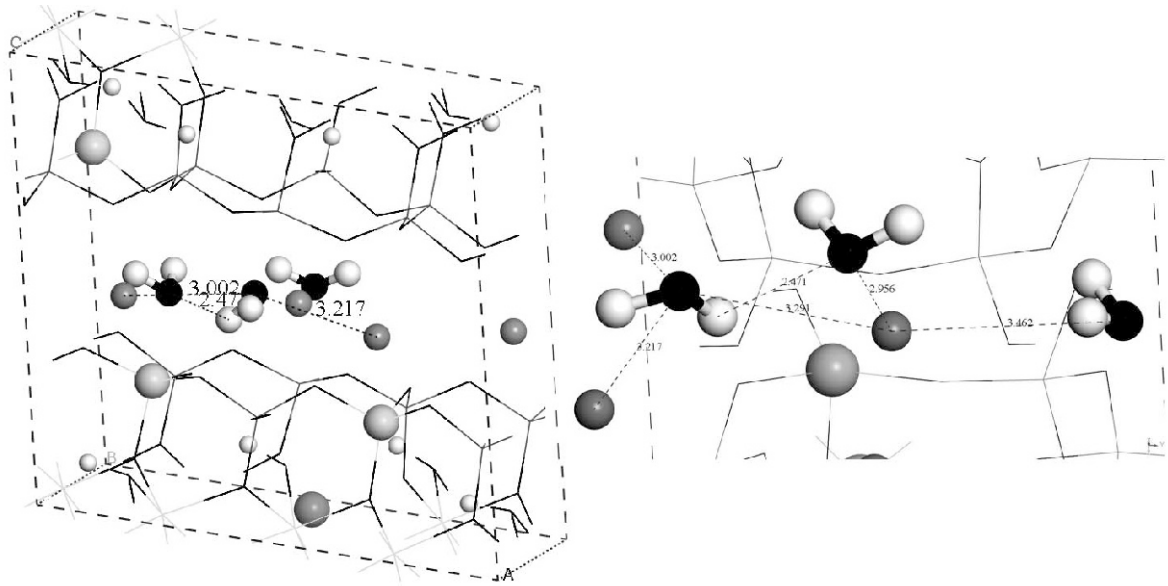

Figure 3. Optimized structure of hydrated illite (K_4w_3 model). The water molecules are highlighted as spheres. Some interatomic distances (Å) are included.

1.4 water-hydronium molecules per $2 \times 1 \times 1$ supercell. Some highly bonded water remains close to the hydronium cations or the amount of hydronium is greater. This may indicate that the water/hydronium ratio would be lower than in the model above ($H_2O/H_3O^+ = 3$).

A structural formula, closer to the experimental one, $K_{0.7}(Si_{3.44}Al_{0.56})(Al_{1.53}Fe^{3+}_{0.19}\ Fe^{2+}_{0.06}Mg_{0.28})O_{10}(OH)_2$, can be considered, therefore, with a lower water/hydronium ratio than above. Hence, a new model closer to this experimental composition was created in a $5 \times 1 \times 1$ supercell with six water molecules distributed homogeneously between ICs, seven K^+, and three hydronium cations per supercell $K_7(H_3O^+)_3(Si_{33}Al_7)(Al_{17}Mg_3)O_{100}(OH)_{20}(H_2O)_6$, $K_7(H_3O)_3w_6$, where the ratio H_2O/H_3O^+ is 2. After the full optimization of this structure, two hydronium cations remained in the interlayer space and one H_3O^+ was dissociated, transferring a H atom to the hydrophilic SiOAl site, producing a Brönsted site SiOHAl as in the previously described $K_3(H_3O)w_3$ model (Figure 5). The new SiOHAl and water molecule remain interconnected, forming a complex with a long SiO−H bond, d(SiO−H) = 1.08 Å, and a short H bond d(SiOH...OH_2) = 1.41 Å. In all models the Si−OH bond distance is in the range 1.68−1.69 Å, a value which agrees with previous models of hydrated clays (1.69 Å) (Boulet *et al.*, 2006).

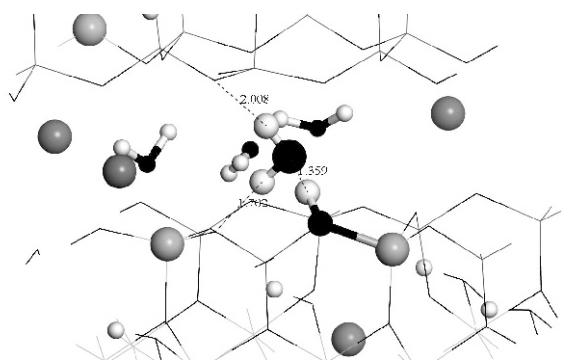

Figure 4. Optimized structure of hydrated illite with hydronium cations in the interlayer space ($K_3H_3Ow_3$ model). The hydronium cations and water molecules are highlighted as spheres. Some interatomic distances (Å) are included.

Two H_3O^+ remain in the interlayer space with different interaction types. One is in the center of the hexagonal cavity with all H atoms oriented toward basal O atoms of the tetrahedral sheet; the hydrogen bonds play an important role because of several interactions observed, the average distance is 2.14 Å ($H_2OH...O_{bT}$), consistent with previous theoretical values reported in acid montmorillonite, 2.14 Å (Liu *et al.*, 2013). As expected, the strongest hydrogen bond is located in an AlOSi site, d($H_2OH...Ob_{TAl}$) = 1.39 Å; previously this site was found to be hydrophilic and to have affinity to protons. This behavior has been observed in several theoretical studies (Boulet *et al.*, 2006; Leydier *et al.*, 2015). The other hydronium is in the center of the interlayer space, interacting with both tetrahedral sheets through hydrogen bonds ($H_2OH...O_{bT}$), the average d ($H_2OH...O_{bT}$) distance is 1.63 Å with a strong hydrogen bond ($H_2OH...O_{bT}$) of 1.34 Å with a basal AlOSi site.

With respect to water molecules, five have interactions with hydrophobic sites of the tetrahedral sheet, *i.e.* electrostatic interactions with SiOSi, the average interaction distance (Si...OH_2) of 1.97 Å; this interaction is possible when oxygen atoms of water are oriented

https://doi.org/10.1346/CCMN.2016.0640406 Published online by Cambridge University Press

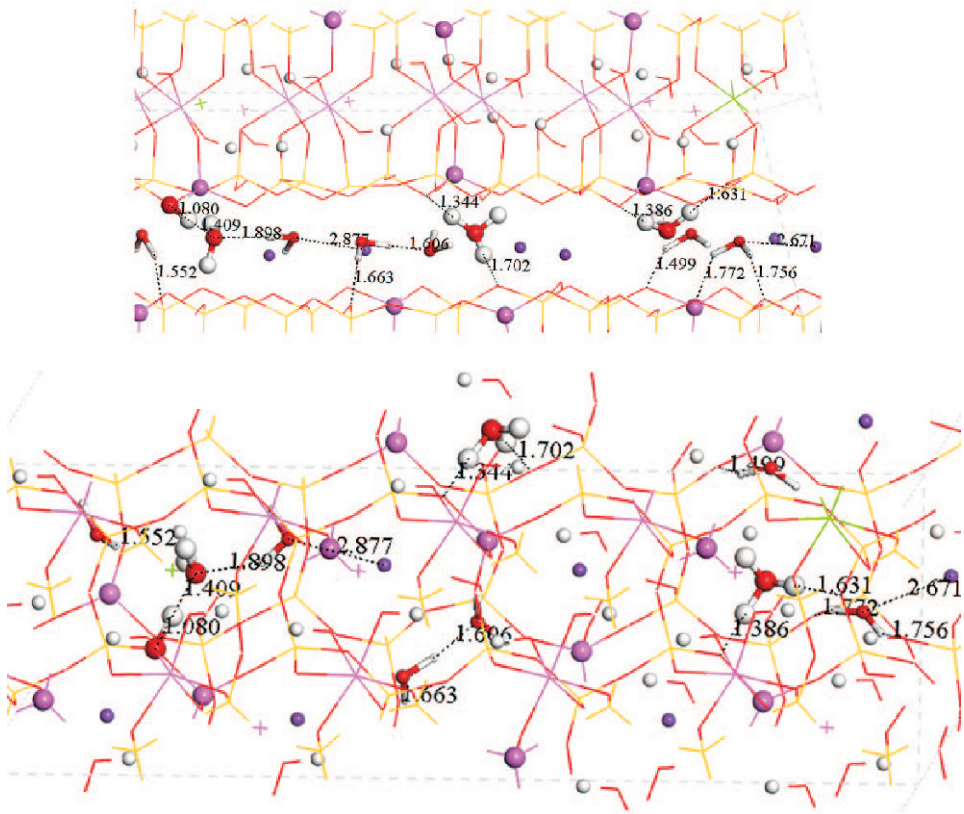

Figure 5. Optimized structure of the supercell of hydrated illite with hydronium cations, $K_7(H_3O)_3w_6$ model (views from the (010) [upper] and (001) [lower] planes). The H, Al, Mg, Si, O, and K atoms are represented by white, pink, green, yellow, red, and purple colors, respectively. The tetrahedral Al^{3+} and K^+ cations and water atoms are shown as spheres. The hydronium atoms are highlighted as larger spheres. Some interatomic distances (Å) are included.

toward the Si^{4+} cation of the tetrahedral sheet. The opposite occurs when the H atoms of a water molecule are oriented toward basal O atoms by strong hydrogen bonds; the average distance is 1.70 Å (HOH...ObT).

Seven IC (K^+) together with solvating water molecules were placed in the center of the interlayer space. The average (K...OH_2) distance was 3.06 Å, slightly shorter than K...OH in the previous hydrated model. Intermolecular interactions between water–water and water–hydronium molecules were observed, with an average distance *d*(O...H) of 2.01 and 2.54 Å, which corresponds to the electrostatic interactions H_2O....H_2O and H_3O^+....H_2O, respectively. These (H_3O....H_2O) interaction distances are consistent with previous calculations on solvated hydronium (2.5 Å) (Brorsen *et al.*, 2014).

Cation exchange process

In order to simulate the cation exchange process between K^+ and hydronium cations in the interlayer space of illite, an additional model was created to trap the cation placed outside the interlayer space after the cation exchange. The cation, K^+ or H_3O^+, was placed in the center of a sphere of 20 water molecules neutralized with one HO^- anion. The stabilization energy, ΔE_s, can thus be defined as:

$$\Delta E_s = (E_{ilK3hyd} + E_{Kwater}) - (E_{ilK4} + E_{hydwater})$$

where $E_{ilK3hyd}$ is the energy of illite with potassium and hydronium cations; E_{Kwater} is the energy of K^+ within the water ball; E_{ilK4} is the energy of illite with only potassium cations at the IC position; and $E_{hydwater}$ is the energy of the hydronium cation within the water ball.

In all models with hydronium cations and without water molecules, the calculated stabilization energy indicated that the stability of H_3O^+ in the interlayer space needs intake energy in relation to its presence in aqueous solution. The stabilization energy ΔE_s of the model K_3H_3Oa is 11.7 kcal/mol. This means that the hydration energy is greater than the exchange energy. This approach can be extended to the above model of a $5 \times 1 \times 1$ supercell with some water molecules surrounding the IC, $K_7(H_3O^+)_3(Si_{33}Al_7)(Al_{17}Mg_3)O_{100}(OH)_{20}(H_2O)_6$. The ΔE_s of this partially hydrated model is 10.2 kcal/mol (extrapolated to the $2 \times 1 \times 1$ supercell). Taking into account the models with three water molecules, K_4w_3 and $K_3H_3Ow_3$, where the amount of water is close to the experimental one, the stabiliza-

https://doi.org/10.1346/CCMN.2016.0640406 Published online by Cambridge University Press

tion energy ΔE_s is 1.49 kcal/mol, confirming the significance of the hydration energy.

Hence, a model with IC in a greater hydration state, similar to that in the water ball, should be created. Then, an additional model was generated where the interlayer space hydronium cation is solvated with four water molecules in a solvation coordination similar to the water sphere, $(Si_{13}Al_3)(Al_7Mg)K_3(H_3O^+)(OH)_8O_{40}(H_2O)_4$. With this model the stabilization energy ΔE_s was −8.89 kcal/mol. This means that with a similar hydration energy, the hydronium cation is more stable in the interlayer space of illite than outside. To corroborate this result, an additional model was generated with a $2 \times 1 \times 1$ supercell with 12 water molecules in the interlayer space distributed homogeneously between the IC with c = 12.0 Å. This model creates a large degree of hydration of interlayer hydronium for comparison with the external water medium, but does not reproduce swelling effects in illites, which do not occur in nature. In this model, the exchange of one K^+ cation by a hydronium cation is exothermic (ΔE_s = −9.4 kcal/mol) which means that the hydronium cation is also more likely to be at the center of the interlayer space than K^+. This ΔE_s value is more negative than the former model with four water molecules per hydronium cation. In this last model, the degree of hydration can be considered as constant before adsorption, where the hydronium is coordinated with 20 water molecules; after adsorption, the hydronium in the interlayer space is coordinated with 12 water molecules. The last value of ΔE_s corresponds to the cation exchange of K^+ by a hydronium ion.

These results support the suggestion that the hydronium is stable in the interlayer space. Any illite can, therefore, be compensated easily with hydronium cations coming from the water solution, this process being energetically favorable. This hydronium will remain in the interlayer space after the drying process due to the strong H bonds between the hydronium H atom and the tetrahedral basal O atoms.

Spectroscopic properties

IR spectra. Experimental IR spectra of the illite IMt-2 sample with different water contents (Figure 6) revealed in all cases that the main peaks were in the range 1150 to 800 cm^{-1}, corresponding to the structural vibrations of the Si−O, Al−O bonds. In this complex band, some peaks can be distinguished around 920 and 800 cm^{-1} which can be assigned to the bending in-plane δ(OH) vibration mode of OH groups of the octahedral sheet of AlOHAl and AlOHMg, respectively (Figure 6a). These bands remain unchanged irrespective of the amount of water. Another band of low intensity can be observed at 3600 cm^{-1}, assigned to the stretching vibration mode ν(OH) of the OH groups from the octahedral sheet. This band has a certain width (3700−3550 cm^{-1}) and can include other coupled bands of ν(OH) from OH groups of the octahedral sheet, AlOHAl and AlOHMg groups with different local environments, as seen below (Ortega-Castro *et al.*, 2008; 2009). A wide, broad band in the range 3500−2800 cm^{-1} is assigned to the ν(OH) vibration mode of the water molecules and hydronium cation. This wide range is the convolution of several bands of OH groups, the vibrations of which have different frequencies due to different H bonds and electrostatic interactions with other molecules or tetrahedral O atoms, as explained in the calculated spectroscopic properties given below. This is consistent with previous studies on hydrated micaceous minerals with a broad band at 3450−2600 cm^{-1} (White and Burns, 1963). Another interesting band appears at 1740−1590 cm^{-1}, which can be assigned to the bending vibration mode of OH groups, δ(OH) (scissors), of water and hydronium moieties. This band is asymmetric with a shoulder at 1740−1680 cm^{-1} that can be assigned to the δ(OH) of the hydronium cation (Figure 6b). The maximum of this band at 1630 cm^{-1} can be assigned to the δ(OH) of water molecules. This is consistent with the bending band of water molecules detected previously in montmorillonite at 1630 cm^{-1}, which showed a completely symmetric band (Xu *et al.*, 2000), in contrast to this work. Previous IR spectra of hydrated micaceous minerals with hydronium cations showed bands at 1750−1700 cm^{-1} (White and Burns, 1963) in accordance with the present results. The weak bands observed at 1450−1360 cm^{-1} can be assigned to the bending vibration of OH groups (umbrella mode) of hydronium cations (Figure 6b).

After heating for 24 h at 175ºC (Figure 6c), the band of the octahedral OH groups remained and the intensity of the broad band in the range 3500−3000 cm^{-1}, assigned to the ν(OH) of water molecules, decreased drastically due to the loss of water. This broad band can also include a ν(OH) band of the hydronium cation at 3450 cm^{-1}, consistent with previous studies which found this band at 3472 cm^{-1} for hydronium cation in muscovite (*e.g.* White and Burns, 1963). In this broad band, two overlapped bands can be detected at 2930 and 2850 cm^{-1}, which can be assigned to ν(OH) vibrations of silanol groups or water molecules with strong H bonds and also the OH groups from the edge surfaces. The δ(OH) bands of the hydronium cation and water molecules can now be distinguished more clearly here at 1740 and 1640 cm^{-1}, respectively. Nevertheless, vibrations of water molecules forming H bonds with hydronium cations can be included in this range according to previous works on micaceous minerals (White and Burns, 1963). The umbrella δ(OH) bands at 1450−1360 cm^{-1} remain as above, though the relative intensity is greater than before, indicating overlap with a δ(SiO−H) band of silanol groups and the $\delta(OH)_{umbrella}$ of hydronium groups, as found theoretically (see below).

After heating the sample at 220ºC for 24 h (Figure 6d), no further dehydration was detected though the relative intensity of the band at 1490−1380 cm^{-1}

https://doi.org/10.1346/CCMN.2016.0640406 Published online by Cambridge University Press

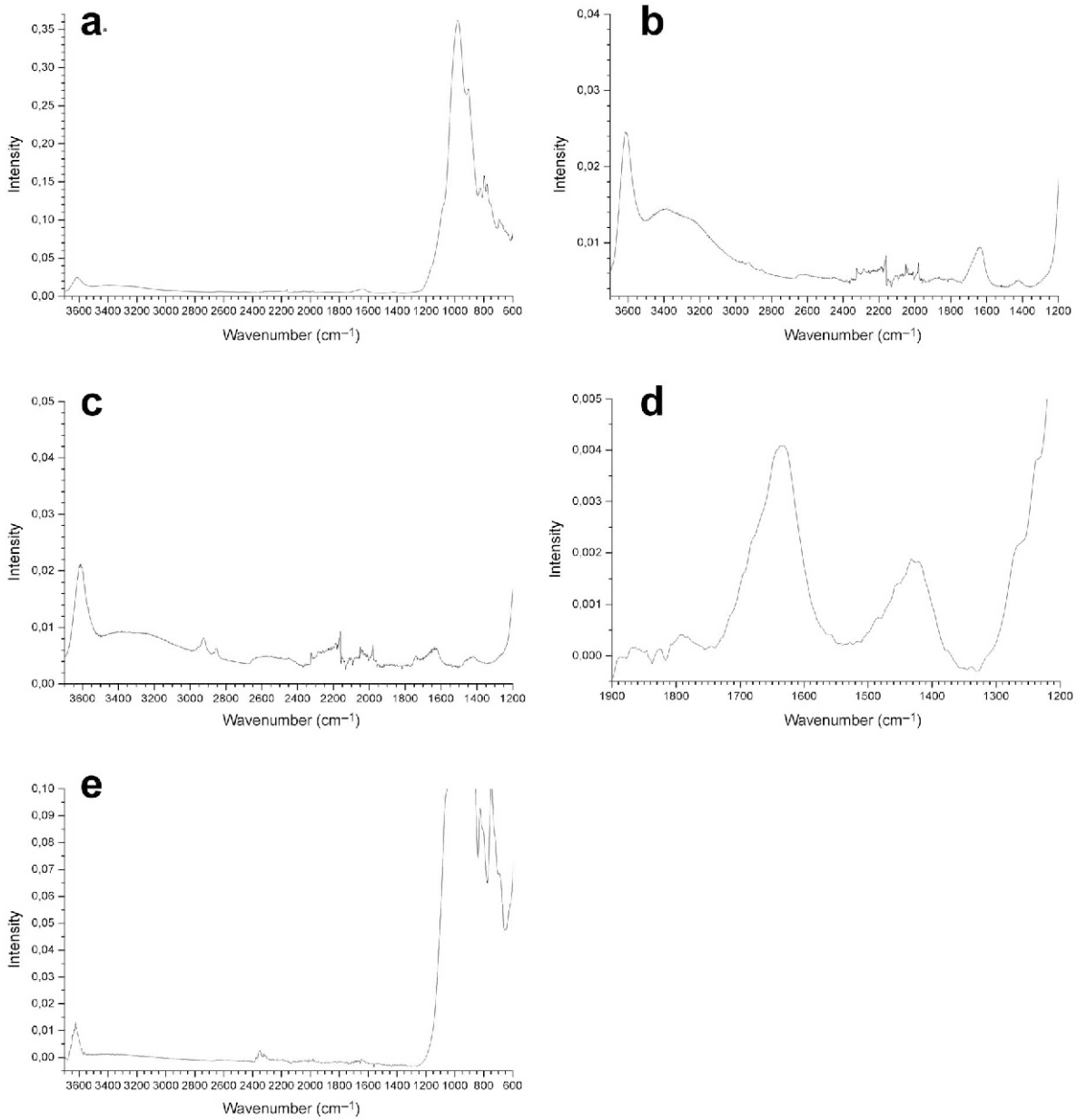

Figure 6. Experimental IR spectra of the illite sample: at 45% moisture (a, b); and heated at 175ºC (c) and 220ºC (d); and of a pegmatitic mica (e).

(assigned to δ(SiO−H) and $\delta(OH)_{umbrella}$ of hydronium from the calculations below) increased in relation to the 1700−1600 cm^{-1} band. This can be explained by a larger number of silanol groups formed during the dehydration or the existence of hydronium groups and a further partial rehydration in the handling process (Figure 6d).

These results were compared with the spectrum of a pegmatitic mica heated to 100ºC, where no vibration bands related to water molecules or to a hydronium cation were found, confirming the above assignments (Figure 6e).

Calculated frequencies

The main spectroscopic properties of phyllosilicates which are related to cation arrangements are those of the OH groups of the octahedral sheet. In the present calculations, the main vibration normal modes can be distinguished directly because mainly the H and O atoms of OH groups participate in the atomic displacements of the normal coordinates for these vibrations, especially ν(OH), distinguishing the stretching vibration mode ν(OH), ranging from 3800 to 3655 cm^{-1}, the in-plane deformation mode δ(OH) at 950−650 cm^{-1}, and the out-of-plane deformation mode γ(OH) (650−450 cm^{-1}).

https://doi.org/10.1346/CCMN.2016.0640406 Published online by Cambridge University Press

This latter frequency range is difficult to detect experimentally due to overlap with SiO vibration bands that are always present in these types of minerals. The wide frequency range of these bands is due to the types of cation joined to the OH groups and the different local environment of each OH. AlOHAl and AlOHMg groups can be distinguished. The probability of finding a MgOHMg is very small due to the low relative concentration of Mg and the high energy of this cation arrangement found in previous calculations (Sainz-Díaz *et al.*, 2003). The OH groups can have different local environments, in any case, due to the relative positions of tetrahedral Al cations and the octahedral Mg cations, and the interlayer cations with respect to each OH. This difference in the relative position produces a gradient of charge distribution in the tetrahedral O atoms surrounding the OH groups, changing the ρ angle (angle of the OH bond with the 001 plane) and also the interaction with the OH bond during the ν(OH) vibration mode and, hence, the frequency according to previous studies (Ortega-Castro *et al.*, 2008). This phenomenon was detected experimentally (Tokiwai and Nakashima, 2010) in muscovite. The effect exists to varying extents for all vibration modes ν(OH), δ(OH), and γ(OH).

Considering the average frequencies, the ν(AlOHMg) vibration appears at greater frequency than the ν(AlOHAl) mode, in agreement with a previous experimental report (Russell and Fraser, 1971). The relationship between experimental and calculated frequencies is not linear because of the differences between the actual chemical compositions of the natural samples and the models. Nevertheless, at room temperature, the OH groups can oscillate due to the thermal vibration varying permanently the ρ angle. Hence, the observed ν(OH) frequency is not related directly to ρ but rather to the effects of the whole environment surrounding each OH group and no discrete bands will be observed but, instead, a broad band at 3700−3550 cm^{-1}. In general, the effect of the isomorphous substitutions of octahedral cations on calculated ν(OH) frequencies is consistent with experimental spectra and previous works (Table 2) (Fialips *et al.*, 2002).

The calculated ν(OH) bands of the water and hydronium molecules appear in the range 3756−2833 cm^{-1} according to the experimental values (3500−2800 cm^{-1}). The frequency variation of the ν(OH) modes of the OH groups of these molecules will depend on the strength of the H-bond interactions around their local environment. Hence, the ν(OH) bands of those OH groups with stronger H bonds will appear at lower frequency, especially for the hydronium cations strongly bound with water molecules that appear at 2828 (in K_3H_3Oa) and 2376 (in $K_3H_3Ow_{12}$) cm^{-1}. This vibration mode of the dissociated hydronium cation appears at 2052 cm^{-1}.

The bending δ(OH) bands of scissor mode appear at 1713 and 1677 cm^{-1} in the dry model with hydronium cation. These bands are also observed in the hydrated models and in the experimental analysis. The other bending mode, $\delta(OH)_{umbrella}$, appears at 1379 cm^{-1} in the dry K_3H_3Oa complex and at 1249 cm^{-1} in the wet $K_3H_3Ow_{12}$ sample (Table 2). This indicates that this vibration mode has to overcome the external interactions during the atomic movement, and then stronger intermolecular interactions will yield higher frequencies in δ(OH). This is corroborated by the great difference between this δ(OH) frequency and that calculated for the free hydronium cation in the gas phase where no external interaction is present (908 cm^{-1}). In the partially hydrated $K_3H_3Ow_3$ model, the δ(OH) bands of the partially dissociated hydronium-silanol complex appear at 1466−1386 cm^{-1} in accordance with the experiments

Table 2. Frequencies of the main vibration modes of illite in dry (K_3H_3Oa) and hydrated ($K_3H_3Ow_{12}$ and $K_3H_3Ow_3$, respectively) models compared with experimental data.

Mode (cm^{-1})	Exp.	K_3H_3Oa	$K_3H_3Ow_{12}$	$K_3H_3Ow_3$
$\nu(OH)_{octa}$	3700−3550	3766−3697	3800−3660	3812−3655
$\nu(OH)_{H_2O}$	3500−2800 3450−2600[c]	3330 3590−3585[a]	3756−3104, 3300−3100[b]	3563−2833
$\nu(OH)_{H_2OH...OT}$	3472−3450[c]	2828, 2052	3034−2630, 2376	
$\delta(OH)_{scissor}$	1740−1590, 1750−1700[c]	1713, 1677 1656−1652[a]	1620[b], 728−1607	1697−1564,
$\delta(OH)_{umbrella}$, H_3O^+	1450−1360	1379, 908[a]	1249	1466−1386
ν(SiOH)	2930, 2850	2808[d]		1564
δ(SiOH)	1450−1360			1466−1386, 1311[d]

[a] Calculated value for H_3O^+ in the gas phase (Demontis *et al.*, 2013).
[b] Calculated value of solvated hydronium (Baer *et al.*, 2011).
[c] From H_3O^+/micas (White and Burns, 1963).
[d] δ(SiOH) (Escamilla-Roa and Moreno, 2012, 2013).

https://doi.org/10.1346/CCMN.2016.0640406 Published online by Cambridge University Press

presented above. δ(SiOH) or δ(H_2OH) could not be differentiated, because both groups form the complex. Nevertheless, the δ(SiOH) mode of this model appears at a greater frequency than in free silanol groups of other systems reported in previous calculations of forsterite (Escamilla-Roa and Moreno 2012, 2013), because in this model the silanol groups form a strong H bond with hydronium cations.

CONCLUSIONS

Spectroscopic studies show that, compared to water molecules, the hydronium cation remains in the interlayer space of illites at higher temperatures. This is due to the tetrahedral charge generated by the Al substitution. The more negatively charged basal O atoms of the tetrahedral sheet interact strongly with hydronium cations. This is corroborated by quantum mechanical calculations which have found that the hydronium cation is likely to be in the interlayer space.

Calculated vibration spectra frequencies reveal that in the interlayer space of illite, with tetrahedral charge, the hydronium cations and water molecules interact strongly with basal O atoms through H bonds. The hydronium cation can form a complex with Si−O forming a quasi-silanol group with a H bridging atom. This effect was also observed experimentally, when heating some samples.

All these quantum mechanical calculations and IR spectroscopic results conclude that the existence of hydronium cations, or Si-O-H groups, should be considered in the calculation of formulae of all illite samples as a possible compensation mechanism for the deficit of charge linked to interlayer charge.

ACKNOWLEDGMENTS

The authors are grateful to the 'Centro Técnico de Informática' of CSIC and to the 'Centro de Supercomputación de la Universidad de Granada' for allowing use of their computational facilities. The present study was supported by the Andalusian projects RNM363 and RNM1897 and the National MINECO project FIS2013-48444-C2-2-P.

REFERENCES

Accelrys (2009) Accelrys Inc. Materials Studio, San Diego, California, USA.

Baer, M., Marx, D., and Mathias, G. (2011) Assigning predissociation infrared spectra of microsolvated hydronium cations $H_3O^+(H_2O)n$ (n = 0, 1, 2, 3) by ab initio molecular dynamics. *ChemPhysChem*, **12**, 1906−1915.

Benco, L. and Tunega, D. (2009) Adsorption of H_2O, NH_3 and C_6H_6 on alkali metal cations in internal surface of mordenite and in external surface of smectite: a DFT study. *Physics and Chemistry of Minerals* **36**, 281−290.

Bishop, J.L., Pieters, C.M., and Edwards, J.O. (1994) Infrared spectroscopic analyses on the nature of water in montmorillonite. *Clays and Clay Minerals* **42**, 702−716.

Boulet, P., Greenwell, H.C., Stackhouse, S., and Coveney, P.V. (2006) Recent advances in understanding the structure and reactivity of clays using electronic structure calculations. *Journal of Molecular Structure: Theochem*, **762**, 33−48.

Brorsen, K.R., Pruitt, S.R., and Gordon, M.S. (2014) Surface affinity of the hydronium Ion: The effective fragment potential and umbrella sampling. *Journal of Physical Chemistry B*, **118**, 14382−14387.

Brown, G. and Norrish, K. (1952) Hydrous micas. *Mineralogical Magazine*, **29**, 929−932.

Demontis, P., Masia, M., and Suffritti, G.B. (2013) Water nanoconfined in clays: the structure of Na vermiculite revisited by ab initio simulations. *Journal of Physical Chemistry C*, **117**, 15583−15592.

Drits, V.A., Plançon, A., Sakharov, B.A., Besson, G., Tsipurski, S.I., and Tchoubar, C. (1984) Diffraction effects calculated for structural models of K-saturated montmorillonite containing different types of defects. *Clay Minerals*, **19**, 541−561.

Escamilla-Roa, E. and Moreno, F. (2012) Adsorption of glycine by cometary dust: Astrobiological implications. *Planetary and Space Science*, **70**, 1−9.

Escamilla-Roa, E. and Moreno, F. (2013) Adsorption of glycine on cometary dust grains: II − Effect of amorphous water ice. *Planetary and Space Science* **75**, 1−10.

Escamilla-Roa, E. and Sainz-Díaz, C.I. (2014) Effect of amorphous ammonia−water ice onto adsorption of glycine on cometary dust grain and IR spectroscopy. *Journal of Physical Chemistry C*, **118**, 26080−26090.

Escamilla-Roa, E., Hernández-Laguna, A., and Sainz-Díaz, C.I. (2013) Cation arrangement in the octahedral and tetrahedral sheets of cis-vacant polymorph of dioctahedral 2:1 phyllosilicates by quantum mechanical calculations. *American Mineralogist*, **98**, 724−735.

Escamilla-Roa, E., Hernández-Laguna, A., and Sainz-Díaz, C.I. (2014) Theoretical study of the hydrogen bonding and infrared spectroscopy in the cis-vacant polymorph of dioctahedral 2:1 phyllosilicates. *Journal of Molecular Modeling*, **20**, 1−15.

Fialips, C.I., Huo, D., Yan, L., Wu, J., and Stucki, J.W. (2002) Infrared study of seduced and reduced-reoxidized ferruginous smectite. *Clays and Clay Minerals* **50**, 455−469.

Giese, R. (1979) Hydroxyl orientations in 2:1 phyllosilicates. *Clays and Clay Minererals* **27**, 213−223.

Hower, J. and Mowatt, T.C. (1966) The mineralogy of illites and mixed-layer illite/montmorillonites. *American Mineralogist*, **51**, 825−854.

Kuligiewicz, A., Derkowski, A., Szczerba, M., Gionis, V., and Chryssikos, G.D. (2015) Revisiting the infrared spectrum of the water-smectite interface. *Clays and Clay Minerals*, **63**, 15−29.

Leydier, F., Chizallet, C., Costa, D., and Raybaud, P. (2015) Revisiting carbenium chemistry on amorphous silica-alumina: Unraveling their milder acidity as compared to zeolites. *Journal of Catalysis*, **325**, 35−47.

Liu, X., Lu, X., Sprik, M., Cheng, J., Meijer, E.J., and Wang, R. (2013) Acidity of edge surface sites of montmorillonite and kaolinite. *Geochimica et Cosmochimica Acta*, **117**, 180−190.

Michot, L.J., Ferrage, E., Jiménez-Ruiz, M., Boehm, M., and Delville, A. (2012) Anisotropic features of water and ion dynamics in synthetic Na- and Ca-smectites with tetrahedral layer charge. A combined quasielastic neutron-scattering and molecular dynamics simulations study. *Journal of Physical Chemistry C*, **116**, 16619−16633.

Morrow, C.P., Yazaydin, A.O., Krishnan, M., Bowers, G.M., Kalinichev, A.G., and Kirkpatrick, R.J. (2013) Structure, energetics, and dynamics of smectite clay interlayer hydration: Molecular dynamics and metadynamics investigation of Na-hectorite. *Journal of Physical Chemistry C*, **117**, 5172−5187.

Nieto, F., Mellini, M., and Abad, I. (2010) The role of H_3O^+ in the crystal structure of illite. *Clays and Clay Minerals*, **58**, 238–246.

Ortega-Castro, J., Hernández-Haro, N., Hernández-Laguna, A., and Sainz-Díaz, C.I. (2008) DFT calculation of crystallographic properties of dioctahedral 2:1 phyllosilicates. *Clay Minerals*, **43**, 351–361.

Ortega-Castro, J., Hernández-Haro, N., Muñoz-Santiburcio, D., Hernández-Laguna, A., and Sainz-Díaz, C.I. (2009) Crystal structure and hydroxyl group vibrational frequencies of phyllosilicates by DFT methods. *Journal of Molecular Structure: Theochem*, **912**, 82–87.

Perdew, J.P., Burke, K., and Ernzerhof, M. (1996) Generalized gradient approximation made simple. *Physics Review Letters*, **77**, 3865.

Rieder, M., Cavazzini, G., D'yakonov, Y.S., Frank-Kamenetskii, V.A., Gottardi, G., Guggenheim, S., Koval, P.V., Mueller, G., Neiva, A.M.R., Radoslovich, E.W., Robert, J.-L., Sassi, F.P., Takeda, H., Weiss, Z., and Wones, D.R. (1998) Nomenclature of the micas. *Clays and Clay Minerals*, **46**, 586–595.

Russell, J. and Fraser, A. (1971) IR spectroscopic evidence for interaction between hydronium ions and lattice OH groups in montmorillonite. *Clays and Clay Minerals*, **19**, 55–59.

Sainz-Díaz, C.I., Hernández-Laguna, A., and Dove, M.T. (2001) Theoretical modelling of cis-vacant and trans-vacant configurations in the octahedral sheet of illites and smectites. *Physics and Chemistry of Minerals*, **28**, 322–331.

Sainz-Díaz, C.I., Palin, E.J., Dove, M.T., and Hernández-Laguna, A. (2003) Monte Carlo simulations of ordering of Al, Fe, and Mg cations in the octahedral sheet of smectites and illites. *American Mineralogist*, **88**, 1033–1045.

Sainz-Díaz, C.I., Escamilla-Roa, E., and Hernández-Laguna, A. (2005) Quantum mechanical calculations of trans-vacant and cis-vacant polymorphism in dioctahedral 2:1 phyllosilicates. *American Mineralogist*, **90**, 1827–1834.

Tokiwai, K. and Nakashima, S. (2010) Integral molar absorptivities of OH in muscovite at 20 to 650ºC by in-situ high-temperature IR microspectroscopy. *American Mineralogist*, **95**, 1052–1059.

Wang, J., Kalinichev, A.G., Kirkpatrick, R.J., and Cygan, R.T. (2005) Structure, energetics, and dynamics of water adsorbed on the muscovite (001) surface: A molecular dynamics simulation. *Journal of Physical Chemistry B*, **109**, 15893–15905.

White, J.L. and Burns, A.F. (1963) Infrared spectra of hydronium ion in micaceous minerals. *Science*, **141**, 800–801.

Xu, W., Johnston, C.T., Parker, P., and Agnew, S.F. (2000) Infrared study of water sorption on Na, Li, Ca, and Mg-exchanged (SWy-1 and SAz-1) montmorillonite. *Clays and Clay Minerals*, **48**, 120–131.

(*Received 26 November 2015; revised 17 May 2016; Ms. 1072; AE: A. Kalinichev*)